1521-0111/91/4/416–427$25.00
MOLECULAR PHARMACOLOGY

http://dx.doi.org/10.1124/mol.116.106633
Mol Pharmacol 91:416–427, April 2017

Sequence-Specific Regulation of Endocytic Lifetimes Modulates Arrestin-Mediated Signaling at the μ Opioid Receptor[S]

Zara Y. Weinberg, Amanda S. Zajac, Tiffany Phan, Daniel J. Shiwarski, and Manojkumar A. Puthenveedu

Department of Biological Sciences, Center for the Neural Basis of Cognition, Carnegie Mellon University, Pittsburgh, Pennsylvania

Received January 13, 2017; accepted January 30, 2017

ABSTRACT

Functional selectivity at the μ opioid receptor (μR), a prototypical G-protein–coupled receptor that is a physiologically relevant target for endogenous opioid neurotransmitters and analgesics, has been a major focus for drug discovery in the recent past. Functional selectivity is a cumulative effect of the magnitudes of individual signaling pathways, e.g., the $G\alpha_i$-mediated and the arrestin-mediated pathways for μR. The present work tested the hypothesis that lifetimes of agonist-induced receptor-arrestin clusters at the cell surface control the magnitude of arrestin signaling, and therefore functional selectivity, at μR. We show that endomorphin-2 (EM2), an arrestin-biased ligand for μR, lengthens surface lifetimes of receptor-arrestin clusters significantly compared with morphine. The lengthening of lifetimes required two specific leucines on the C-terminal tail of μR. Mutation of these leucines to alanines decreased the magnitude of arrestin-mediated signaling by EM2 without affecting G-protein signaling, suggesting that lengthened endocytic lifetimes were required for arrestin-biased signaling by EM2. Lengthening surface lifetimes by pharmacologically slowing endocytosis was sufficient to increase arrestin-mediated signaling by both EM2 and the clinically relevant agonist morphine. Our findings show that distinct ligands can leverage specific sequence elements on μR to regulate receptor endocytic lifetimes and the magnitude of arrestin-mediated signaling, and implicate these sequences as important determinants of functional selectivity in the opioid system.

Introduction

Although canonically called G-protein–coupled receptors (GPCRs), GPCRs can signal through diverse pathways after ligand binding (Pierce et al., 2002; Belcheva et al., 2005; DeWire et al., 2007). GPCR activation by ligands induces conformational changes, allowing initial signaling through G-proteins (Pierce et al., 2002) and phosphorylation by G-protein–coupled receptor kinases, generating a phosphorylation barcode that is recognized by β-arrestins (Premont and Gainetdinov, 2007; Nobles et al., 2011). Arrestins are important effectors of GPCRs outside of G proteins, modulating both their trafficking and signaling (Goodman et al., 1996; Shenoy and Lefkowitz, 2011). Arrestins scaffold diverse downstream kinases, including Src and extracellular signal-regulated kinases 1 and 2 (ERK1/2), on activated GPCRs to initiate G-protein–independent signaling (Luttrell et al., 1999; DeWire et al., 2007; Shenoy and Lefkowitz, 2011).

Signaling bias between G-protein and arrestin-dependent pathways is an area of increasing interest in pharmacology (Urban et al., 2007; Lefkowitz et al., 2014; Zhou and Bohn, 2014). This functional selectivity, or biased agonism, has therapeutic potential, as specific pathways are being linked to specific physiologic effects (Law et al., 2013; Chang and Bruchas, 2014; Kenakin, 2015; Luttrell et al., 2015;). Functional selectivity is relevant, especially in the field of opioid physiology. The μ receptor (μR), the primary target of most clinically relevant analgesics, can signal via both G-proteins and arrestins to cause complex physiologic effects (Raehal et al., 2011; Williams et al., 2013; Thompson et al., 2015). Initial indications for functional selectivity came when morphine was shown to cause poor arrestin recruitment and

This research was supported by the National Institutes of Health National Institute on Drug Abuse [Grant DA024698], National Institute of General Medical Sciences [Grant GM117425], and the National Science Foundation [Grant 117776] to M.A.P. Z.Y.W. was partially supported by the National Institutes of Health National Institute of Neurologic Disorders and Stroke [Grant T32 NS007433], and D.J.S. was partially supported by a DeVries Fellowship to Carnegie Mellon University.
dx.doi.org/10.1124/mol.116.106633.
[S] This article has supplemental material available at molpharm.aspetjournals.org.

ABBREVIATIONS: 2-AG, 2-arachidonoylglycerol; AUC, area under the curve; CB1R, cannabinoid 1 receptor; CCP, clathrin-coated pit; cEKAR, cytosolic-localized ERK kinase activity report; CFP, cerulean fluorescent protein; DAMGO, [D-Ala2, *N*-MePhe4, Gly-ol]-enkephalin; DMEM, Dulbecco's modified Eagle's medium; DMSO, dimethylsulfoxide; EM2, endomorphin-2; EPAC, exchange protein directly activated by cAMP; ERK1/2, extracellular signal-regulated kinases 1 and 2; FBS, fetal bovine serum; FRET, Förster resonance energy transfer; GPCR, G-protein–coupled receptor; LLAA μR, μR with L389 and L392 mutated to A; nEKAR, nuclear-localized ERK kinase activity report; PDZ, postsynaptic density-95/disc-large/zona occludens (PSD-95/Dlg/ZO-1); pERK, phospho-ERK; μR, μ receptor; siRNA, short-interfering RNA; SSF, signal sequence/FLAG; TIR-FM, total internal reflection fluorescence microscopy; WIN 55,212-2, (11R)-2-methyl-11-[(morpholin-4-yl)methyl]-3-(naphthalene-1-carbonyl)-9-oxa-1-azatricyclo[6.3.1.$0^{4,12}$]dodeca-2,4(12),5,7-tetraene; WT, wild type.

internalization compared with endogenous opioids (Keith et al., 1996; Sternini et al., 1996; Whistler and von Zastrow, 1998). This was substantiated by arrestin knockout in mice, which attenuated a subset of physiologic effects of opioids (Raehal et al., 2011; Thompson et al., 2015). Recently, biased μR ligands that separate the beneficial and adverse effects of opioids have shown great therapeutic potential (Violin et al., 2014; Manglik et al., 2016). Importantly, ligand bias is a function of the strengths of each signaling pathway, and the absolute magnitude of each pathway determines the downstream effects. This raises the possibility that the bias of a given drug can be controlled by changing the magnitude of individual pathways through which it signals.

The mechanisms by which ligands bias μR signaling are not clear. Research has focused on conformational changes and post-translational modifications that change the affinity of arrestin-μR interactions (Yu et al., 1997; Azzi et al., 2003; Rivero et al., 2012; Bradley and Tobin, 2016). It is evident, however, that the subcellular location of receptors is equally important, as it can significantly change the downstream effectors to which receptors couple (Ferrandon et al., 2009; Jean-Alphonse et al., 2014; Tsvetanova and von Zastrow, 2014; Bowman et al., 2016). Whether and how receptor trafficking influences functional selectivity of opioids is still unexplored.

In this context, μR and arrestin interact primarily in well defined endocytic domains in cells. After arrestin recruitment, μR-arrestin complexes either recruit the endocytic protein clathrin or are translocated to clathrin-coated pits (CCPs) (Whistler and von Zastrow, 1998; Wolfe and Trejo, 2007; Shenoy and Lefkowitz, 2011). This is followed by a highly ordered process of growth, maturation, and scission of the CCP, termed clathrin-mediated endocytosis (McMahon and Boucrot, 2011; Taylor et al., 2011; Traub and Bonifacino, 2013; Cocucci et al., 2014). GPCRs themselves can directly modulate clathrin-mediated endocytosis dynamics (Puthenveedu and von Zastrow, 2006; Henry et al., 2012; Soohoo and Puthenveedu, 2013; Flores-Otero et al., 2014; Lampe et al., 2014). μR actively regulates CCP scission via short amino acid motifs in its C-terminal intracellular tail (Soohoo and Puthenveedu, 2013), but the roles of these novel sequence elements in regulating μR function are not known.

Here, we tested the hypothesis that these sequence elements determine the magnitude of arrestin signaling and, therefore, functional selectivity of μR by regulating the dynamics of receptor endocytosis. Our results show that endomorphin-2 (EM2), an arrestin-biased ligand for μR, lengthens surface lifetimes significantly compared with morphine. This regulation required a specific sequence on the C-terminal tail of μR. Sequence-dependent lengthening of lifetimes was required for arrestin-biased signaling by EM2. Lengthening surface lifetimes by independently slowing endocytosis was sufficient to increase the magnitude of arrestin signaling, but not G-protein signaling. Our findings implicate receptor surface lifetimes, controlled by a specific bileucine sequence on the μ receptor, as an important factor in regulating arrestin signaling without changing G-protein signaling in the opioid system.

Materials and Methods

Cell Culture and DNA Constructs. All experiments were performed with HEK 293 cells (American Tissue Culture Collection, Manassas, VA). Cells were cultured in Dulbecco's modified Eagle's medium (DMEM; Fisher Scientific, Waltham, MA) with 10% fetal bovine serum (FBS; Thermo Scientific, Waltham, MA). All plasmid transfections were conducted with Effectene (Qiagen, Hilden, Germany) per the manufacturer's instructions. Receptor constructs signal sequence/FLAG–μR (SSF-μR), supercliptic phluorin–μR, supercliptic phluorin–μR–LLAA, and SSF-μR-LLAA were all described previously (Soohoo and Puthenveedu, 2013). Stable cell lines expressing one of the aforementioned constructs were generated using Geneticin (Thermo Scientific) as selection reagent. Cytosolically-localized ERK kinase activity report (cEKAR) was a gift from Oliver Pertz [Addgene plasmid #39835 (Fritz et al., 2013)], and nuclear-localized ERK kinase activity report (nEKAR) was generated from that plasmid by EcoRV restriction digest followed by religation to remove the nuclear export signal. β-Arrestin2 tagged with green fluorescent protein (GFP) was previously described (Puthenveedu and von Zastrow, 2006). The exchange protein directly activated by cAMP (EPAC) sensor for cAMP concentration sensor has been previously described (DiPilato et al., 2004). Endomorphin-2 and morphine (Sigma-Aldrich, St. Louis, MO) were prepared as 10 mM stocks in sterile water and used at 10 μM. Dynasore (Sigma-Aldrich) was prepared as 40 mM stock in dimethylsulfoxide (DMSO) and used at 40 μM. Knockdown of β-arrestin1 and β-arrestin2 was conducted using 50 pmol of four pooled short-interfering RNA (siRNA) sequences targeted to each isoform (cat. nos. L-007292-00-0005 and L-011971-00-0005; GE Dharmacon, Lafayette, CO) and cotransfected with EKAR sensors using Lipofectamine (Thermo Scientific). Control siRNA (sequence: GACCAGCCATCGTAGTACTTT) was synthesized using an Ambion siRNA Silencer Construction Kit (Thermo Scientific). Arrestin knockdown was assessed using pan-arrestin antibody (cat. no. PA1-730, used at 1:1000; Pierce Protein Biology, Rockford, IL), with lysates run on a stain-free 4–20% gradient SDS-PAGE gel (Bio-Rad, Hercules, CA) and stain-free images taken to ensure equal load before transferring to nitrocellulose membrane.

EKAR Förster Resonance Energy Transfer Assays. Cells stably expressing a construct of μR were transfected with either cEKAR or nEKAR (300 ng). Cells were passed to coverslips, then imaged 2–3 days post transfection at roughly 50% confluency. Prior to imaging, cells were serum starved for 4 hours by removing growth medium, washing gently with Dulbecco's phosphate buffered saline twice, and then adding 1 ml of L-15 medium. Cells were incubated with Alexa647-conjugated M1 antibody (Thermo Scientific; Sigma-Aldrich) for 10 minutes to label SSF-μR. Cells were imaged at 37°C using an Eclipse Ti automated inverted microscope with a 60×/1.49 Apo-TIRF objective (Nikon Instruments, Melville, NY). Cells were excited using 405- or 647-nm solid-state lasers, and every 30 seconds, images were collected for cerulean fluorescent protein (CFP) (405-nm excitation, 470/50 emission filter), Förster resonance energy transfer (FRET; 405-nm excitation, 530lp emission filter), and Alexa647 (647-nm excitation, 700/75 emission) using an iXon+ 897 EMCCD camera (Andor, Belfast, UK). Cells were incubated with serum-free medium for 5 minutes to establish baseline FRET response and then stimulated with drug for 25 minutes. Images were exported as 16-bit tiff stacks and analyzed in ImageJ (National Institutes of Health, Bethesda, MD). Images were automatically thresholded, and then the FRET channel was used to generate a cell mask. Images underwent a Gaussian blur (sigma = 2px) to remove heterogeneity in signal introduced by delay between CFP and FRET channel correction, and then FRET channel was divided by CFP channel for each frame to determine the FRET ratio. All resulting ratios were normalized to an average ratio during baseline, and all values displayed here are a measure of fractional increase in FRET ratio over baseline.

EPAC FRET Assays. Cells stably expressing μR were transfected with EPAC sensor (300 ng) and imaged 2 days later. To allow for maximal cAMP production, cells were preincubated for 2 hours prior to imaging in L-15 medium containing 1% FBS and 300 μM 3-isobutyl-1-methylxanthine to inhibit phosphodiesterase activity. Imaging was conducted as described earlier. After imaging for 5 minutes to establish a baseline, cells were exposed to 1 μM forskolin to induce

maximal cAMP production, and then 5 minutes later, EM2 was added. Analysis was conducted as described earlier, except that the calculated ratios given the in the paper are CFP/FRET.

Surface Lifetime Assays. Cells stably expressingμR was transfected with β-arrestin2 tagged with green fluorescent protein (100 ng) and imaged 2–3 days later. Imaging used the same setup as described earlier; however, this time, a Nikon TIRF module. Cells were selected for imaging based on minimal initial visible arrestin fluorescence to increase signal-to-noise ratio of arrestin puncta. Images for arrestin (488-nm excitation, 525/50 emission) and the receptor (647-nm excitation, 700/75 emission) were taken every 3 seconds. Cells were allowed to equilibrate to imaging conditions for 1 minute before drug addition. Images were analyzed manually in ImageJ by tracking puncta between frames to determine their surface lifetime—a spot was only considered for manual analysis if its appearance and disappearance could be clearly visualized and it underwent minimal lateral movement. Images also underwent automated analysis, utilizing the cmeAnalysisPackage available from the Danuser Laboratory (Dallas, TX. Previously described in Aguet et al., 2013) with minor updates to allow compatibility with newer versions of MATLAB (MathWorks, Natick, MA) (all code with modifications available at https://github.com/exark/cmeAnalysisPackage). The arrestin channel was used as the master, and all lifetimes reported are based on category I, II, and V tracks as detected by the software, as these categories were required to include all previously manually identified tracks.

Phospho-ERK1/2 Blots. Cells stably expressing either wild type (WT) or LLAA μR were plated at a density of $3.33 \times 10^4/cm^2$ and allowed to grow overnight in DMEM with 10% FBS. Cells were starved in serum-free DMEM for 4 hours prior to lysis. Cells were pretreated with either dynasore (40 μM) or DMSO for 20 minutes before drug addition. After drug treatment, cells were incubated the for stated period of time, then placed on ice and lysed and scraped in the plate with 2X RSB (Bio-Rad, Hercules, CA). Lysates were run on 4–20% stain-free gels, and stain-free images to total protein load were acquired before overnight transfer from gel to the nitrocellulose membrane. Membranes were blocked in 5% bovine serum albumin (Sigma-Aldrich, St. Louis, MO) and then probed for phospho-ERK1/2 (cat. no. 4370, used at 1:1000; Cell Signaling Technology, Danvers, MA). After blots were developed, they were subsequently stripped for 3 hours, then reblocked with 5% milk and probed for total ERK1/2 levels (cat. no. 4695, used at 1:1000; Cell Signaling Technology). Densitometry was calculated in Image Laboratory (Bio-Rad). Each lane's phospho-ERK (pERK) signal was normalized to its total ERK signal, and then normalized to no-treatment condition. Normalized replicates were averaged and are reported as group means ± S.E.M.

Statistical Analyses. All boxplots displayed in figures are displayed as boxes from the 25th quartile to the 75th quartile, with a line for the median, and the minimum and maximum are displayed at the ends of the whiskers. Graphs with a single bar for each group are reported as the mean ± standard error of the mean. For EKAR experiments, all calculations were conducted using Prism 6 (GraphPad Software, La Jolla, CA). Individual cells were included in these analyses if they showed at least three consecutive data points during the treatment with a consistent increase over the average baseline measurement. Peak response values are taken as the maximum value during the treatment phase of the trial. Area under the curve (AUC) is calculated for the treatment phase of the trial, using 1.0 as a baseline measure. AUCs from individual cells were averaged to establish group means. Statistical comparisons for data presented in boxplots were conducted using Mann-Whitney U tests, and comparisons for data displayed in bar graphs was done using a t test with Welch's correction. Comparisons of peak and AUC data were evaluated against a Šidák-corrected P value of 0.0253 to keep familywise error at less than 5% for these multiple comparisons. Comparisons where analysis of variance was used are specifically noted, with post-hoc comparisons between the means of indicated groups having been conducted to test for significance.

For clustering experiments, manual surface lifetime measurements were averaged to produce population means, and means were compared with two sample t tests with Welch's correction in Prism. The fraction of clusters with lifetimes greater than 150 seconds was averaged across cells and is reported as group means ± S.E.M. Cumulative distributions of clusters with lifetimes greater than 150 seconds from automated analysis were compared using a two-sample Kolmogorov-Smirnov test for distribution independence using the function kstest2 in MATLAB, with the corresponding P value and KS statistic reported.

Results

Endomorphin-2 Induces Longer Surface Lifetimes of Receptor-Arrestin Clusters and Greater Arrestin-Mediated ERK1/2 Activation Compared with Morphine. We hypothesized that, if the time the receptor spends at the cell surface after agonist treatment (surface lifetime) colocalized with arrestin affects arrestin-mediated signaling magnitude, we should see disparate lifetimes in ligands depending on the magnitude of arrestin recruitment that a ligand was capable of producing. EM2 was selected as an example of an endogenous ligand for μR that is able to strongly recruit arrestin (Rivero et al., 2012), and morphine was selected as a model ligand with a demonstrated ability to poorly recruit arrestin to the receptor (Zheng et al., 2008; McPherson et al., 2010; Raehal et al., 2011).

To investigate the magnitude of arrestin-dependent signaling produced by these two ligands, we assayed for ERK1/2 activation, a well documented downstream effector of arrestin (Luttrell and Lefkowitz, 2002; DeWire et al., 2007). HEK 293 cells stably expressing a construct of the murine μR with an N-terminal FLAG epitope were treated with saturating concentrations (10 μM) of either EM2 or morphine for 5 minutes and then lysed. Subsequent immunoblotting revealed a subtle but significant increase in ERK1/2 phosphorylation for EM2 treatment compared with morphine (Supplemental Fig. 1). To achieve better temporal and spatial sensitivity, we used the FRET biosensor EKAR (Fritz et al., 2013) to assay for ERK1/2 activation in live cells. The same cell line used for immunoblotting was transiently transfected with either cEKAR and nEKAR. Cells were labeled with an Alex647-conjugated M1-FLAG antibody and then imaged live to visualize receptor internalization and FRET ratio changes following agonist treatment (Fig. 1, A, B, G, and H).

Both in the nucleus and in the cytosol, ERK activity peaked about 5 minutes after agonist addition for both agonists (see Fig. 1, C and I for example traces). EM2 produced a greater peak ERK1/2 response in both the nucleus and the cytosol (Fig. 1, D and J). The same trend of greater EM2-elicited activation compared with morphine was seen when measuring total ERK1/2 response by taking the area under the curve of each response, with EM2 producing a greater total response than morphine in both cytosol and nucleus (Fig. 1, E and K). In the cytosol, the difference in total ERK response was more pronounced than in the nucleus due to a second phase of ERK activation that was only present for EM2 and not for morphine (Fig. 1I). This is consistent with prior data which suggest that arrestin signaling induces a temporally distinct wave of ERK signaling.

To assess the contribution of arrestin-dependent signaling to the difference in ERK1/2 activation between morphine and

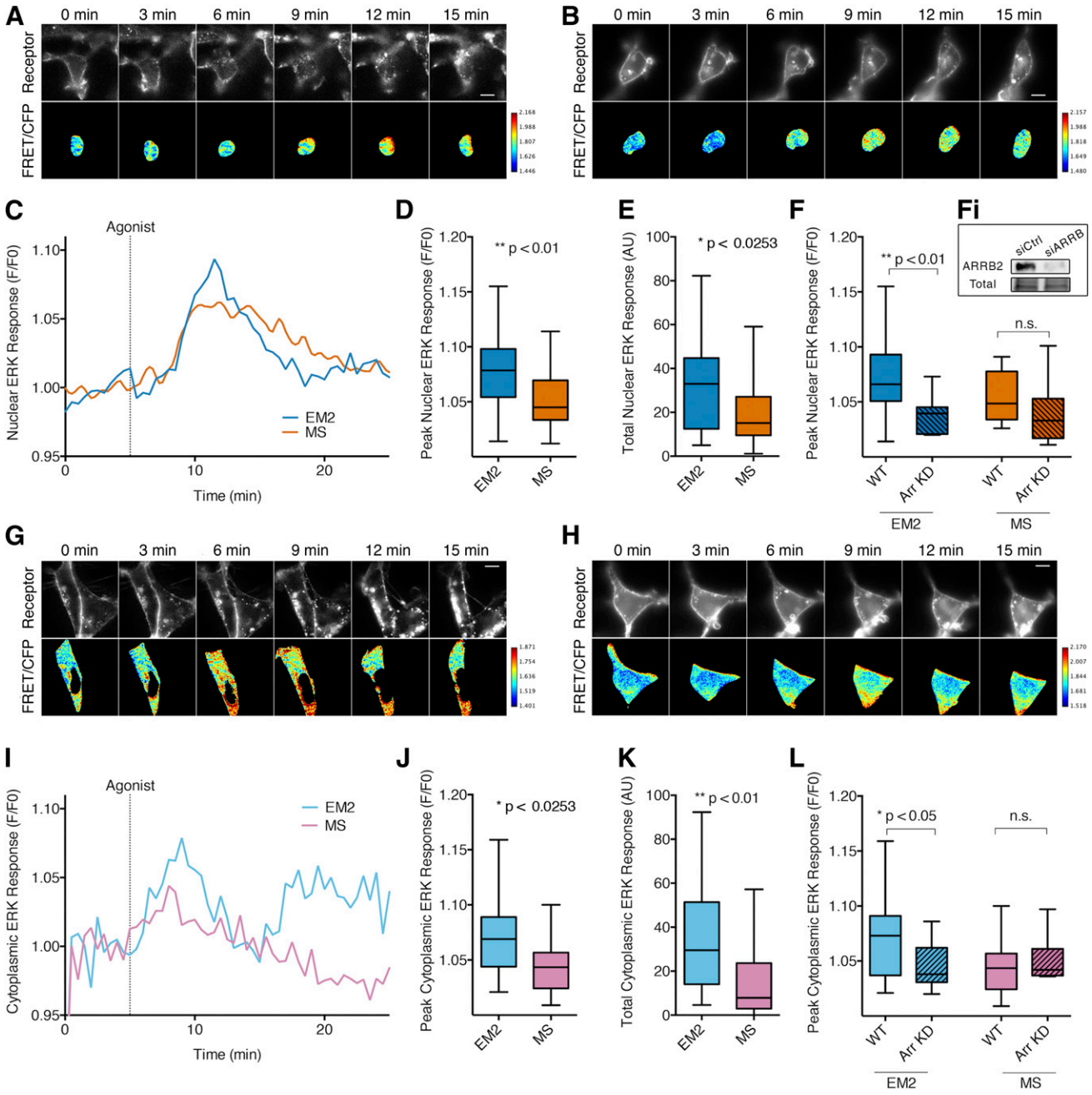

Fig. 1. Morphine and endomorphin-2 have distinct arrestin signaling profiles at WT μR. (A) Example montage of nuclear EKAR response in WT μR–expressing cells in response to EM2. (Top row) FLAG-tagged μR labeled with Alexa647-conjugated M1 antibody. (Bottom row) Ratio of FRET/CFP fluorescence of expressed nEKAR sensor. Agonist added at 5 minutes. Scale bar is 10 μM, frames every 3 minutes. (B) Representative montage of nEKAR response measured in WT μR–expressing cells in response to morphine. (C) Representative traces of nEKAR FRET/CFP ratio for cells treated with either morphine or EM2. A higher amplitude and narrower peak is observed for EM2 compared with morphine. (D) EM2 induces a significantly greater peak amplitude compared with morphine (n = 33 and 25, respectively; $^{**}P < 0.01$). (E) EM2 produces overall greater ERK response compared with morphine, using area under the curve after agonist treatment to assay total ERK response (n = 33 and 25; $^{*}P < 0.0253$). (F) Knockdown (KD) of β-arrestin1/2 significantly decreases peak ERK response for EM2-treated cells (n = 24 and 10 for control and knockdown, respectively; $^{**}P < 0.01$) but does not significantly change the peak for morphine-treated cells [n = 12 and 7, not significant (n.s.)]. (Fi) Knockdown confirmation, with intense bands from stain-free total protein of the same gel as control. (G) Example montage for cEKAR sensor response to EM2, presented in the same manner as (A). (H) Representative montage of cEKAR response to morphine. (I) Representative traces for cytosolic ERK activation for morphine and EM2. (J) EM2-dependent peak cytosolic ERK response is significantly higher than morphine (n = 53 and 12; $^{*}P < 0.0253$). (K) Total ERK response for EM2 is greater in the cytosol compared with morphine (n = 53 and 12; $^{**}P < 0.01$). (L) β-Arrestin1/2 knockdown again significantly decreases peak ERK signal for EM2 (n = 29 and 10; $^{*}P < 0.05$) while having no effect on morphine peak response (n = 12 and 6, n.s.). Arr, arrestin; AU, arbitrary units; MS, morphine sulfate; siARRB, siRNA targeting β-arrestin1/2; siCtrl, nonsense siRNA.

EM2, we performed a double knockdown of β-arrestin1 and β-arrestin2 and then measured ERK response with EKAR. Knockdown was confirmed via immunoblot, with the arrestin signal normalized to total protein from a stain-free gel image (Fig. 1Fi, see *Materials and Methods* for further details). For EM2, arrestin knockdown significantly decreased peak signaling in the cytosol and in the nucleus (Fig. 1, F and L), with a specific effect of reducing the second peak. Arrestin

knockdown did not have a significant effect on morphine-dependent ERK activation. This suggests that the difference in ERK1/2 activation between these two agonists is primarily controlled by arrestin-dependent signaling.

Given the arrestin dependence of the difference in ERK signaling between morphine and EM2, we investigated whether these agonists induced differential lifetimes of receptor clusters with arrestin. Previous work has demonstrated that clusters of μR that form in response to [D-Ala2, N-MePhe4, Gly-ol]-enkephalin (DAMGO), another endogenous agonist of the receptor, persist at the cell membrane for a protracted duration, with an average lifetime of 100 seconds (Henry et al., 2012; Soohoo and Puthenveedu, 2013). We investigated the extent to which morphine versus EM2 controlled the lifetime of receptor clusters, and specifically whether arrestin colocalized with receptor for the duration of its lifetime.

We imaged HEK 293 cells stably expressing FLAG-μR, transfected with low levels of a green fluorescent protein-tagged β-arrestin2 construct, using total internal reflection fluorescence microscopy (TIR-FM) to visualize arrestin-μR colocalization after agonist addition. For EM2, long-lived receptor clusters were easily visible, and arrestin colocalized with receptor clusters for their entire surface lifetime (Fig. 2A). Similar colocalization was seen with morphine (Fig. 2B). Receptor clustering was also evident in response to morphine,

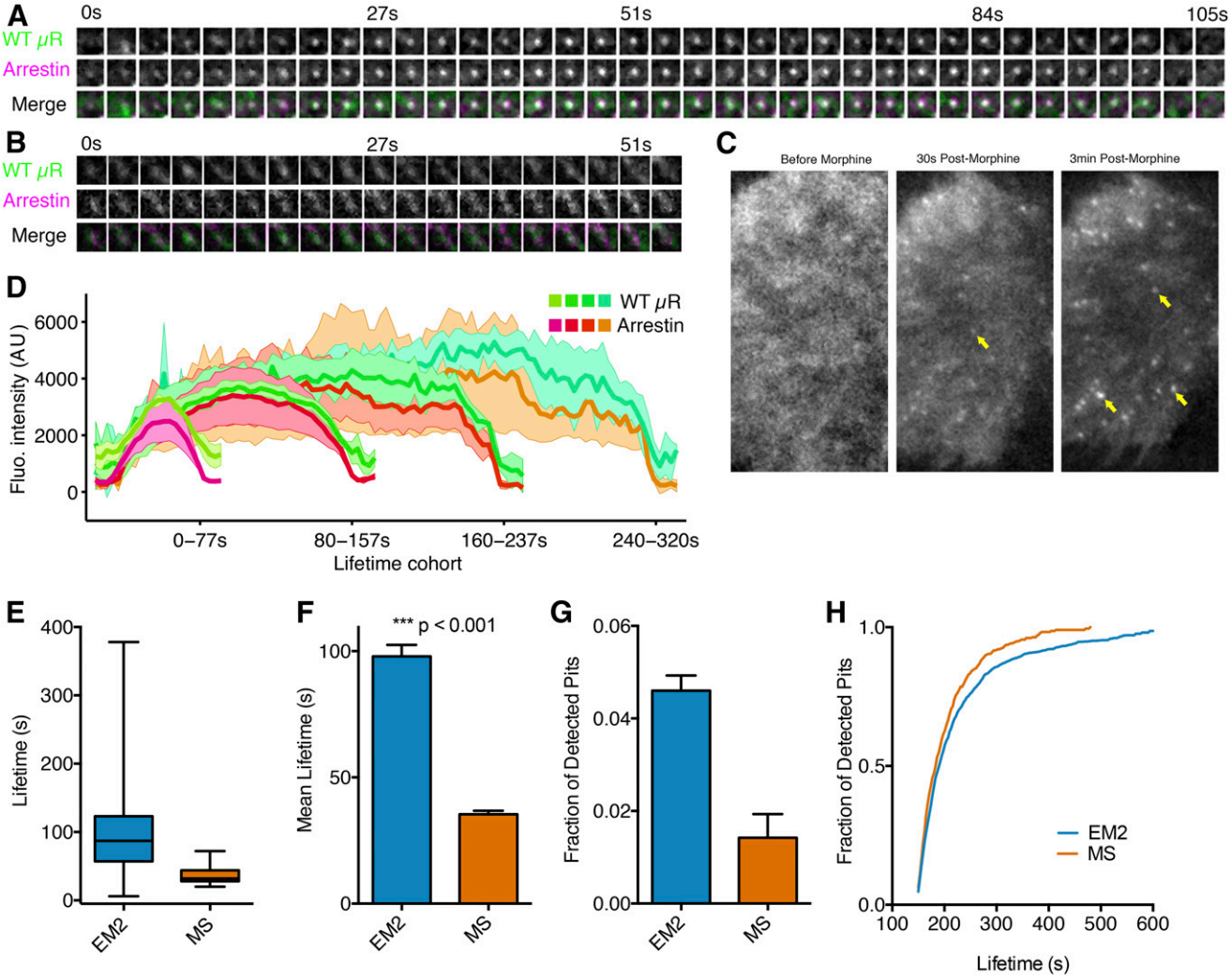

Fig. 2. Arrestin colocalizes with μR clusters for the duration of their endocytic lifetime. (A) Representative montage showing the recruitment timing and colocalization duration for β-arrestin2 with μR in response to EM2. Top row in montage is an Alexa647-labeled FLAG-μR, middle row is a green fluorescent protein-tagged β-arrestin2. Simultaneous fluorescence increases in both channels are seen as well as simultaneous rapid disappearance. (B) Representative montage for arrestin and receptor colocalization after treatment with morphine. (C) Cells expressing WT FLAG-μR and arrestin (shown) before and after morphine treatment. Notable clustering is seen in the arrestin channel rapidly after agonist addition (see arrow in middle column merge), and clusters rapidly disappear with new clusters forming (see difference in identified objects between middle and last columns). Scale bar is 5 μM. (D) Arrestin versus μR fluorescence for tracks across a variety of lifetime cohorts. Clusters analyzed with cmeAnalysis were grouped into four lifetime cohorts (0–77 seconds, n = 1600 clusters; 80–157 seconds, n = 141; 160–237 seconds, n = 16; 241–320 seconds, n = 2). Arrestin intensity at clusters roughly overlaps with receptor fluorescence. (E) Overall population lifetimes of arrestin cluster lifetimes performed through manual quantification. Higher maximum and median cluster lifetimes are seen for EM2 compared with morphine (n = 149 and 73 clusters for EM2 and morphine, respectively). (F) Mean lifetime of arrestin clusters. EM2 induces a significantly higher mean lifetime of arrestin clusters compared with morphine (n = 149 and 73 clusters, respectively; ***$P < 0.001$). (G) Automated quantification of the same movies used for (E) and (F) performed with cmeAnalysis package. The number of clusters with lifetimes greater than 150 seconds is displayed here as a fraction of total clusters detected per cell ± S.E.M. (three cells for EM2, seven cells for morphine, total n = 19,549 and 21,665 for clusters in respective conditions). (H) Empirical distribution functions for observed lifetimes over 150 seconds. Curves originate from distinct cumulative distributions as confirmed by Kolmogorov-Smirnov test (D = 0.333, ***$P < 0.001$). AU, arbitrary units; Fluo., fluorescence, MS, morphine sulphate.

consistent with previous reports on cells expressing arrestin (Whistler and von Zastrow, 1998), with arrestin clusters colocalizing with μR (Fig. 2C). Automated analysis of clustering movies allowed quantification of receptor and arrestin fluorescence over time, with results showing that, regardless of cluster lifetime, arrestin and receptor presence at clusters coincided for the lifetime of the cluster (Fig. 2D). Surface lifetimes of arrestin clusters were measured manually as explained in *Materials and Methods* and as described previously (Puthenveedu and von Zastrow, 2006; Soohoo and Puthenveedu, 2013). The lifetimes of EM2-dependent arrestin clusters were longer compared with morphine. EM2 produced a maximum arrestin cluster lifetime of 378 seconds and a median of 87 seconds compared with a maximum of 72 seconds and median of 32 seconds for morphine (Fig. 2E). Average lifetimes for arrestin clusters across the population were significantly longer for EM2 compared with morphine (97.93 ± 4.501 for EM2 vs. 35.40 ± 1.393), correlating with the difference seen in ERK1/2 activation between the two ligands (Fig. 2F).

We next used an objective and automated image-analysis method to measure surface lifetimes to provide an unbiased analysis of all endocytic clusters across the whole experimental data set. To do this, we adapted an available automated tool set for measuring lifetimes of diffraction limited spots from TIR-FM movies (Aguet et al., 2013) to measure the difference in lifetimes between the two agonists. As reported previously, the absolute values of population dynamics differed from the manual analysis, with the automated analysis identifying a much larger fraction of shorter-lived clusters than were identified through manual methods (Loerke et al., 2009; Liu et al., 2010; Doyon et al., 2011; Aguet et al., 2013; Soohoo and Puthenveedu, 2013; Mettlen and Danuser, 2014; Hong et al., 2015). Nevertheless, the automated analysis recapitulated the longer lifetimes seen for EM2 compared with morphine, particularly evident in a greater frequency of longer-lived pits of above 150 seconds in duration (Fig. 2G). This difference is apparent as an overall rightward shift of the EM2 lifetime cumulative distribution compared with morphine (Fig. 2H).

Lengthened Surface Lifetimes Are Required for Maximal ERK1/2 Signaling by Endomorphin-2. Our aforementioned results indicate that the duration that arrestin colocalizes with μR during internalization correlates with the magnitude of arrestin signaling. To test whether there is a causal relationship between surface lifetime and arrestin signaling, we first asked whether increased EM2 signaling via arrestin required long-lived receptor clusters.

To investigate this, we used a specific mutant of μR (LLAA μR, L389A, L392A) that internalizes quickly and has previously been shown to have a short lifetime in response to DAMGO compared with WT μR (Soohoo and Puthenveedu, 2013). We used TIR-FM to visualize clustering and arrestin-colocalization dynamics of cells stably expressing either WT or LLAA μR treated with EM2. Importantly, EM2-treated LLAA μR behaved similar to morphine-treated WT μR in activation and arrestin recruitment. However, the heterogeneity of the overall lifetimes of arrestin clusters was greatly diminished in the mutant compared with the WT receptor (Fig. 3A). LLAA μR also had a significantly shorter mean lifetime of arrestin clusters after agonist addition (Fig. 3B). Additionally, the automated analysis showed a distinction between WT and LLAA μR, with the WT receptor accruing a greater fraction of arrestin clusters with lengthy lifetimes (Fig. 3C) as well as having a significant rightward shift of its cumulative distribution curve (Fig. 3D). Combined with our earlier data with DAMGO, these data with EM2 indicate that L389 and L392 of μR are required for increasing surface lifetime of receptor-arrestin clusters after activation.

Importantly, there were no differences in overall arrestin recruitment between the WT and LLAA μR. When cells expressing WT or LLAA μR and a tdTomato-tagged β-arrestin2 construct were imaged using TIR-FM with high time resolution (10 Hz), arrestin recruitment appeared comparable across cells (Fig. 3E), with clusters appearing at roughly commensurate times in each cell line. To quantify the kinetics of arrestin recruitment, these movies were analyzed using automated analysis to identify clusters. When fluorescence intensities for individual clusters were measured across many clusters, the time to plateau of cluster fluorescence was uniformly about 6 seconds, and slopes were identical between WT and LLAA μR–expressing cells (Fig. 3F). These results show that the LLAA μR mutant recruited arrestin to comparable levels, but showed shorter surface lifetimes. This provided an excellent model to test whether increased EM2 signaling via arrestin requires long-lived receptor clusters.

To test whether shortened lifetimes changed the magnitude of arrestin-mediated signaling, we measured ERK1/2 activation caused by LLAA μR upon EM2 treatment. Peak ERK1/2 activation was significantly higher for WT μR compared with LLAA μR in the cytosol (cEKAR, Fig. 4A), with the same trend in total response (Fig. 4B). This difference is repeated and accentuated in the nucleus, with WT μR showing a larger increase compared with LLAA μR for both peak and total ERK response (nEKAR, Fig. 4, C and D). The ERK responses of LLAA μR with EM2 were roughly comparable to those of the WT μR with morphine (Fig. 4C vs. Fig. 1C, Fig. 4D vs. Fig. 1H). These results indicate that μR-mediated extension of surface lifetime is required for maximal arrestin-mediated ERK1/2 signaling.

We next tested whether this relationship between surface lifetimes and ERK signaling was conserved across different agonists with different magnitudes of arrestin and G-protein signaling. We selected agonists able to recruit arrestin strongly (EM2, DAMGO), moderately (fentanyl, methadone), and weakly (morphine, oxycodone) (McPherson et al., 2010), and tested the responses of WT and LLAA μR in the EKAR assay. To measure signaling differences, we calculated mean total ERK response (AUC) to each agonist for both WT and LLAA μR. We then subtracted the LLAA mean from the WT mean to determine the difference score, or magnitude of ERK activation difference across the two receptors, as an index of the contribution of surface lifetimes to ERK response. Strikingly, the magnitude of difference between WT and LLAA μR paralleled the abilities of the ligands to recruit arrestin (Fig. 4E), indicating that the contribution of extended lifetimes was restricted to arrestin-mediated signaling.

To directly determine whether changes in lifetimes regulated G-protein–dependent signaling, we compared G-protein responses between WT and LLAA μR after EM2. As μR is $G\alpha_{i/o}$ coupled, we assayed receptor-dependent inhibition of cAMP production using the FRET biosensor EPAC (DiPilato et al., 2004). Cells stably expressing either WT or LLAA μR were transiently transfected with EPAC. Cells were subsequently imaged live (Fig. 4, F and G). Forskolin was used to stimulate cAMP production, and then after 5 minutes, EM2 was added to induce inhibition of cAMP production. EM2 induced a rapid decrease in FRET ratio in the case of both receptors (Fig. 4H for example traces), and the overall

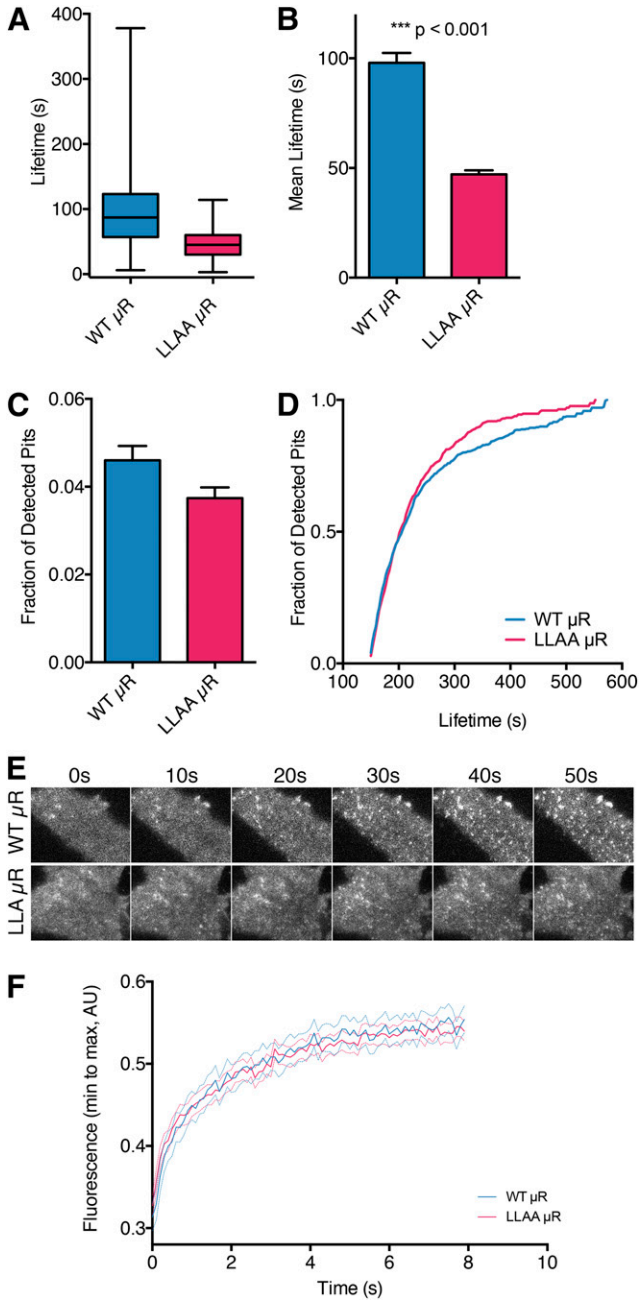

Fig. 3. Mutation of a bileucine sequence in μR C terminus decreases EM2-dependent lifetimes of arrestin clusters but does not affect arrestin recruitment kinetics. (A) Population lifetime distributions for arrestin clusters measured after EM2 addition for WT or LLAA μR (n = 152 and 151 clusters, respectively). (B) Mean lifetimes for arrestin clusters with either WT or LLAA μR. LLAA μR induced significantly shorter overall mean lifetime for arrestin (***$P < 0.001$). (C) Automated quantification was conducted on the same movies analyzed for (A) and (B) using cmeAnalysis. The number of clusters with lifetimes greater than 150 seconds is displayed here as a fraction of total clusters detected per cell ± S.E.M. (three cells for WT μR, three cells for LLAA μR, total n = 19,549 and 26,647 for clusters in respective conditions). (D) Empirical distribution functions for both populations. Curves originate from distinct cumulative distributions as confirmed by Kolmogorov-Smirnov test (D = 0.5854, ***$P < 0.001$). (E) Global arrestin recruitment in cells expressing WT μR (top row) or LLAA μR (bottom row) following EM2 (10 μM) treatment. Cells expressing tdTomato-tagged β-arrestin2 were imaged after agonist treatment at 10 Hz. Formation of initial diffraction-limited clusters can be seen in both cell lines within 10 seconds, with maximal clustering visible within 50 seconds after agonist treatment. (F) Individual arrestin cluster recruitment kinetics were measured using high-speed (10 Hz) imaging. Clusters were analyzed with cmeAnalysis, and then individual cluster fluorescence was normalized from minimum to maximum. Graph shows normalized cluster fluorescence over time (n = 482 clusters for WT, 982 clusters for LLAA), with dashed lines representing 95% confidence interval. AU, arbitrary units.

magnitude of the inhibition was comparable between the two receptor variants (Fig. 4I). These results indicate that WT and LLAA μR have comparable EM2-dependent G-protein activation, showing that, consistent with our model, the differences in surface lifetimes of receptor arrestin clusters specifically drive differences in the ERK1/2 pathway.

Lengthening Surface Lifetimes of Receptor Arrestin Clusters Is Sufficient to Increase μR-Mediated ERK1/2 Signaling. We next determined whether extending lifetimes of LLAA μR was sufficient to increase its ERK1/2 signaling. To test the sufficiency of lengthened lifetimes to increase ERK1/2 signaling, we delayed the endocytosis of LLAA μR by pretreating cells with 40 μM dynasore. Dynasore is a known inhibitor of endocytosis, with previous work showing that ~80 μM final concentration of the drug is enough to block almost 90% of clathrin-mediated endocytic cargo (Macia et al., 2006). As we sought to merely mimic the effects of WT μR and lengthen lifetimes instead of blocking internalization entirely, we used 40 μM dynasore pretreatment to slow endocytic scission. Example kymographs show the increase in lifetimes for LLAA μR (Fig. 5A). We measured an increase in population lifetimes, showing that dynasore treatment had the desired effect in increasing both median lifetime and heterogeneity of population lifetimes for LLAA μR (Fig. 5B).

We next used LLAA to test whether increasing lifetimes was sufficient to increase the magnitude of ERK signaling. We initially attempted to use the EKAR assay to demonstrate changes in ERK activation. In our hands, dynamin inhibitors, such dynasore, produce considerable autofluorescence in the FRET fluorescence channel (Supplemental Fig. 2), which reduced the signal-to-noise ratio enough that we could not detect any differences. We therefore investigated the effects of dynasore on LLAA ERK signaling using an immunoblot to detect pERK. Cells stably expressing LLAA μR were pretreated with either 40 μM dynasore or DMSO as a control for 20 minutes, and then exposed to EM2 for 5 minutes. Cells were subsequently lysed and assayed for pERK1/2 levels. Dynasore pretreatment had no effect on basal ERK1/2 phosphorylation but significantly increased EM2-dependent ERK1/2 activation compared with untreated cells (Fig. 5C). These results indicate that lengthened cluster lifetimes are sufficient to increase ERK1/2 signaling.

Given the results seen with EM2 at the short-lifetime μR mutant, we next tested whether lengthening lifetimes was sufficient to allow morphine to activate ERK1/2 efficiently. In cells pretreated with dynasore, morphine caused higher ERK1/2 activation, as evidenced by higher pERK levels, after 5 minutes. This result shows that lengthened lifetime is sufficient to increase ERK1/2 activation. Together, our data indicate that the lifetime of receptor-arrestin clusters on the cell surface determines the strength of arrestin signaling and, therefore, the functional selectivity of ligands between G-protein and arrestin pathways.

Discussion

Our results show that the μ receptor uses specific sequences on its C terminus to regulate the magnitude of its arrestin-

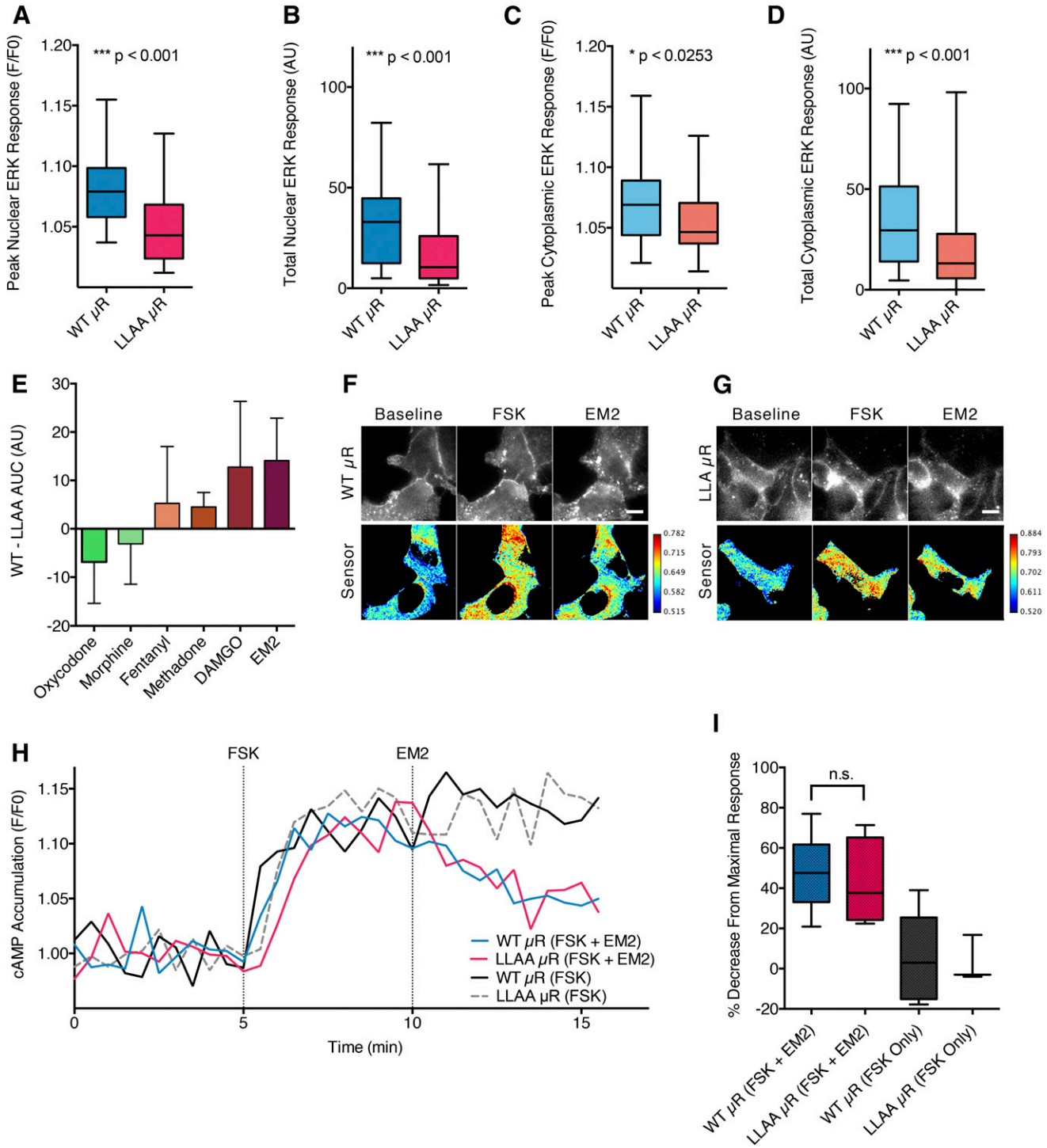

Fig. 4. LLAA μR has diminished ERK activation compared with WT μR, but is equally capable of activating G-protein–dependent signaling. (A) Peak nuclear ERK response as measured by EKAR is much greater for WT μR compared with LLAA μR when both are stimulated by EM2 (n = 33 and 22 for WT and LLAA μR, respectively; $^{***}P < 0.001$). (B) Total ERK response is diminished for LLAA μR compared with WT in the nucleus (n = 33 and 22 for WT and LLAA μR; $^{***}P < 0.001$). The same pattern is seen in the cytosol, with WT μR eliciting a greater peak response compared with the mutant receptor (n = 53 and 40; $^{*}P < 0.0253$) (C) and a higher total ERK response as measured by AUC (n = 53 and 40; $^{**}P < 0.001$) (D). (E) Difference in total ERK response following agonist treatment is dependent on agonist ability to recruit arrestin as described by McPherson et al. (2010). Agonists were all used at 10 μM, and all reported measurements were collected using cEKAR as output for ERK signaling. Mean AUC after treatment of LLAA was subtracted from mean AUC from the same agonist for WT μR, and difference scores are reported here. Error bars represent 95% confidence intervals on difference score (n = 11 and 10 for fentanyl WT and LLAA, respectively; n = 9 and 8 for methadone, 6 and 8 for DAMGO, 11 and 4 for morphine, 53 and 40 for EM2, and 34 and 38 for oxycodone). (F) Example montage of cAMP sensor EPAC in WT μR–expressing cells. From left to right, images show time course for the same cell, each taken 5 minutes apart. Forskolin is added at 5 minutes to stimulate cAMP production, EM2 added at 10 minutes. (Top row) Alexa647-labeled μR. (Bottom row) FRET ratio presented as CFP/FRET fluorescence. Scale bar is 10 μm. (G) Example montage of EM2 ability to inhibit cAMP production in LLAA μR–expressing cells. (H) Example traces from WT μR– or LLAA μR–expressing cells treated with either forskolin followed by EM2, or forskolin alone. (I) Percentage decrease in cAMP production during treatment window, measured as average FRET ratio during forskolin treatment (5–10 minutes) minus average ratio during manipulation (EM2 or

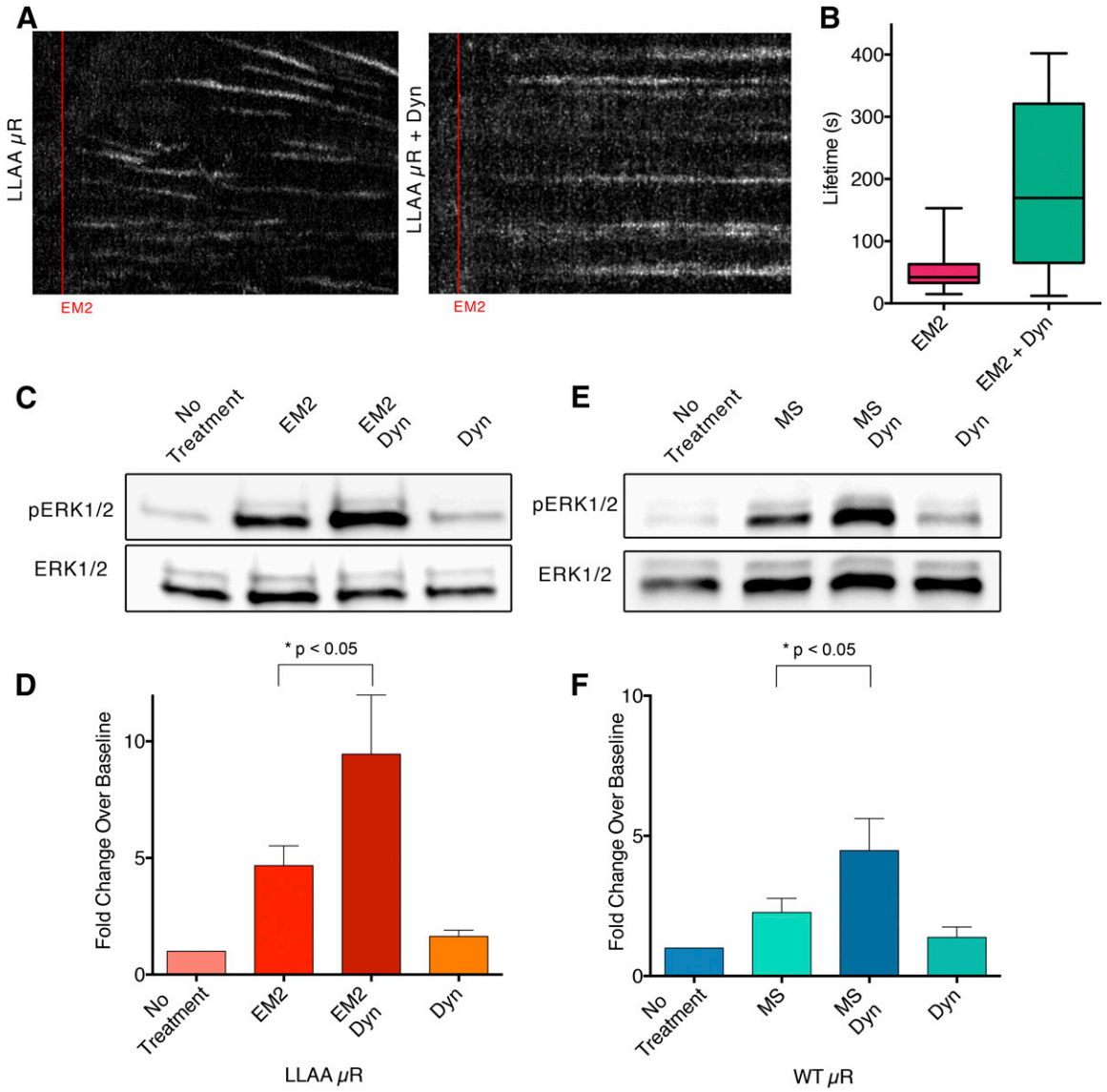

Fig. 5. Extension of endocytic cluster lifetimes with dynasore enhances EM2 signaling at LLAA μR and morphine signaling at WT μR. (A) Kymograph showing lifetimes of LLAA μR clusters (time on x-axis). Each pixel column represents one frame (frames taken every 3 seconds). EM2 added at 1 minute, then imaged for 10 minutes. Left image shows cells pretreated with DMSO. Right image shows cells were pretreated with 40 μM dynasore (Dyn) for 20 minutes before imaging, and dynasore was left in the imaging medium to maintain endocytosis suppression. (B) Boxplot showing difference in population lifetimes in response to dynasore pretreatment (n = 33 and 32 clusters for EM2 and EM2 + dynasore, respectively; $^{***}P < 0.001$). (C) Representative immunoblot for phospho-ERK1/2 in cells expressing LLAA μR and treated with EM2 for 5 minutes and pretreated for 20 minutes with either 40 μM dynasore or DMSO. Top row is phospho-ERK (Thr202), bottom row is ERK1/2 as loading control. (D) Quantification of seven separate blots with no treatment response normalized to 1 for each blot. Dynasore pretreatment increases EM2-dependent ERK response. A significant effect of treatment was seen via a repeated-measures one-way analysis of variance ($^{*}P < 0.05$), with a significant difference seen in post-hoc comparison of dynasore treatment versus DMSO treatment in the presence of EM2. (E) Representative immunoblot of WT μR–expressing cells pretreated with either 40 μM dynasore or DMSO and then treated with morphine for 5 or 10 minutes. (F) Quantification of eight separate blots. Dynasore pretreatment increases total ERK response at 5 minutes. A significant effect of treatment was seen via a repeated-measures one-way analysis of variance ($^{*}P < 0.05$), with a significant difference seen in post-hoc comparison of dynasore treatment versus DMSO treatment in the presence of morphine. MS, morphine sulphate.

mediated signaling by delaying endocytosis and lengthening the lifetimes of receptor-arrestin clusters on the cell surface. Lengthened surface lifetimes were required (Fig. 4, A–D) and sufficient (Fig. 5, A–C) for maximal arrestin signaling from the receptor. The strength of G-protein signaling, in contrast, was not affected by lifetimes (Fig. 4, F–I). This suggests that sequence-dependent regulation of surface lifetimes regulates arrestin signaling at μR without changing G-protein signaling to control functional selectivity.

Surface lifetimes could be a mechanism to tune the functional selectivity of ligands independent of their intrinsic bias. Ligand-dependent differences in the magnitude of arrestin

no additional treatment, 10–15 minutes) divided by maximum response minus baseline (0–5 minutes). A main effect of treatment was seen by one-way analysis of variance ($^{***}P < 0.001$) with Bonferroni post hoc showing no difference between WT and LLAA conditions, but both being significantly different from forskolin (FSK) only ($^{*}P < 0.05$). AU, arbitrary units.

signaling and in functional selectivity at μR are well documented, although the mechanisms are still not well understood (Williams et al., 2013; Raehal and Bohn, 2014). For example, using elegant FRET-based assays, μR was recently shown to cluster in distinct membrane domains on the cell surface in response to ERK EC_{50} doses of morphine (100 nM) and DAMGO (10 nM), leading to differential nuclear and cytoplasmic ERK signaling (Halls et al., 2016). Clustering was not directly tested in these experiments, and our experiments, performed with saturating doses at imaging resolutions that directly detect clustering, resolve the functional nature of these domains. Although 100 nM morphine did not cause nuclear ERK activation (Halls et al., 2016), our experiments with saturating morphine showed nuclear signals, consistent with previous work (Zheng et al., 2008). Interestingly, whereas ERK activation has been linked primarily to cell proliferation and migration (Strungs and Luttrell, 2014), ERK activation in the midbrain or striatum neurons, which are not proliferative, modifies the addictive properties of opioids (Macey et al., 2009; Lin et al., 2010). The differences between experiments may therefore also represent a physiologic divergence of ERK signaling downstream of different agonists.

Different agonists could leverage this ability of surface lifetimes to influence arrestin-mediated signaling. Morphine, a ligand that induces shorter surface lifetimes of μR and arrestin clusters, produces a lower magnitude of arrestin signaling compared with EM2, which induces longer lifetimes (Figs. 1 and 2). Lengthening lifetimes was sufficient to increase the magnitude of arrestin signaling produced by morphine (Fig. 5, E and F). Interestingly, different μR agonists differ in the ability to recruit arrestin (Whistler and von Zastrow, 1998; McPherson et al., 2010; Williams et al., 2013), and this correlated well with the dependence on lifetimes for arrestin signaling, implicating surface lifetime as a modulator of arrestin-dependent signaling (Fig. 4E). It remains unclear whether arrestin itself mediates these extended lifetimes. Our work using the LLAA μR mutant, whose ability to recruit arrestin does not differ from the WT receptor for the same agonist (Fig. 4, E and F), suggests that endocytic delay can be separated from arrestin recruitment. Nevertheless, the differences might be driven by differential μR phosphorylation patterns controlled by different ligands (Tobin et al., 2008; Doll et al., 2011, 2012). It is possible that LLAA, because the C-terminal tail affects receptor phosphorylation patterns (Zindel et al., 2015), shows a different phosphorylation pattern than the WT μR, similar to what is caused by different ligands.

Irrespective of the mechanism, control of surface lifetimes by specific sequences on GPCRs might serve as a general timer for arrestin-mediated signaling from the surface. Such cargo-mediated control of surface lifetimes was first described for the β-adrenoceptors (Puthenveedu and von Zastrow, 2006) and has since been reported for μR and cannabinoid 1 receptor (CB1R) (Henry et al., 2012; Soohoo and Puthenveedu, 2013; Flores-Otero et al., 2014; Lampe et al., 2014). In the case of CB1R, two different ligands—WIN 55,212-2 [(11*R*)-2-methyl-11-[(morpholin-4-yl)methyl]-3-(naphthalene-1-carbonyl)-9-oxa-1-azatricyclo[6.3.1.$0^{4,12}$]dodeca-2,4(12),5,7-tetraene] and 2-AG (2-arachidonoylglycerol)—caused differences in surface lifetimes as well as in arrestin signaling, consistent with our results (Flores-Otero et al., 2014; Delgado-Peraza et al., 2016). The specific mechanisms used, however, might vary between different GPCRs. The β-adrenoreceptors use type I postsynaptic density-95/disc-large/zona occludens (PSD-95/Dlg/ZO-1) domain (PDZ)-ligand sequences on their C termini to lengthen lifetimes by delaying the recruitment of dynamin, a key mediator of endocytic scission (Puthenveedu and von Zastrow, 2006). In contrast, μR uses a bileucine sequence to delay the time to scission after dynamin has been recruited (Soohoo and Puthenveedu, 2013). For the CB1R, recent work suggests that the primary determinant of surface lifetimes is the affinity of arrestin binding itself, dictated by phosphorylation of the receptor (Delgado-Peraza et al., 2016). Although the specific factors used by different receptors to regulate surface lifetimes might differ, the general mechanism likely involves multi-protein interactions that stabilize components of the endocytic machinery.

PDZ domain–containing proteins are attractive candidates to provide a multidomain scaffold for such interactions (Romero et al., 2011; Dunn and Ferguson, 2015). Because PDZ domain–containing proteins can interact with the actin cytoskeleton, and because actin can regulate endocytic dynamics (Grassart et al., 2014; Dunn and Ferguson, 2015), a straightforward possibility is that adrenoceptors regulate endocytosis by recruiting actin or modifying actin dynamics. Consistent with this idea, an actin-binding domain fused to the tail of GPCRs is sufficient to extend surface lifetimes of receptor clusters (Puthenveedu and von Zastrow, 2006). On μR, the bileucine sequence that regulates surface lifetimes and arrestin signaling (Fig. 4, A–D) does not conform to an obvious PDZ ligand sequence, and has no known interactors. This sequence might represent an internal PDZ ligand (Paasche et al., 2005; Lee and Zheng, 2010), although this is unlikely considering that μR delays lifetimes at a step distinct from adrenoceptors. CB1R might also be indirectly linked to PDZ proteins through its binding partner CRIP1 (Daigle et al., 2008; Smith et al., 2015). PDZ interactions are sufficient for regulating surface lifetimes (Puthenveedu and von Zastrow, 2006), but the relative contribution of PDZ interactions and arrestin affinities (Delgado-Peraza et al., 2016) in regulating CB1R endocytosis is not known. A general role for PDZ proteins in regulating functional selectivity is also consistent with reports that PDZ interactions can regulate endocytosis, arrestin recruitment, and ERK signaling by other GPCRs, although whether the effects are through regulating lifetimes is unclear (Yang et al., 2010; Dunn and Ferguson, 2015; Walther et al., 2015; Dunn et al., 2016). However, one key consequence shared between all of these GPCRs is a prolonged interaction between arrestin and receptors on the surface. Arrestins are well recognized regulators of GPCR signaling (Luttrell and Lefkowitz, 2002; Shenoy and Lefkowitz, 2011; Raehal and Bohn, 2014) and trafficking (Goodman et al., 1996), and arrestin-GPCR interactions might be regulated in multiple ways.

These diverse roles of arrestins could result from their ability to adopt a variety of potential conformations and recruit different binding partners, depending on the conformation (Xiao et al., 2007; Gurevich and Gurevich, 2014). Recent work shows that a single receptor can recruit arrestin in a variety of conformations depending on the ligand, leading to distinct signaling profiles (Lee et al., 2016). It is unclear what dictates these conformations, but experiments with chimeric receptors show that the C-terminal tail of a receptor is sufficient. This suggests that amino acid motifs in the

receptor (such as μ opioid receptor's LENLEAE sequence) and/or variable phosphorylation state can modulate arrestin conformation. Since arrestin interacts with endocytic components, conformational variability could determine the composition of the signaling complexes present in endocytic domains. This model also agrees with recent work highlighting new paradigms, where arrestin activation and clustering occur independent of receptor interactions (Eichel et al., 2016), or highly transient receptor-arrestin interactions leave arrestin with a "memory" of activation, leading to arrestin signaling complexes without receptor (Nuber et al., 2016). However, because μR colocalizes well with arrestin throughout the endocytic cycle (Fig. 2, A and B), the effects on arrestin signaling are likely evinced through prolonged association with the receptor.

Although the receptors identified to modulate surface lifetimes so far have been class A receptors, which dissociate from arrestin concomitantly with endocytosis, modulating lifetime might have physiologic consequences even for class B GPCRs, which interact with arrestin for prolonged periods, including on the endosome (Shenoy and Lefkowitz, 2011). Emerging data suggest that the location of signal origin is an important determinant of downstream consequences of GPCR activation. For the β2-adrenoceptor, $G\alpha_s$ signaling from microdomains on the endosome causes the activation of a subset of genes that are distinct from the genes activated by $G\alpha_s$ signaling on the surface (Irannejad et al., 2013; Tsvetanova and von Zastrow, 2014). In the event that a similar paradigm exists for arrestin signaling, surface lifetimes would determine the surface to endosome spatial bias for class B receptors. In this context, our result—that manipulation of receptor surface lifetimes can modulate the magnitude of arrestin signaling—provides a clear example of the potential to control GPCR physiology by manipulating the spatial location of receptors. This is an emerging concept in GPCR biology that builds on the exciting idea that manipulation of receptor location could be a target for developing therapeutic strategies in the future to modulate and fine-tune the diverse effects of existing drugs.

Acknowledgments

The authors thank Drs. Peter A. Friedman, Guillermo G. Romero, Cheng Zhang, Adam D. Linstedt, and Sandra J. Kuhlman for valuable feedback over the course of the project. Members of the M.A.P. Laboratory, particularly Dr. Shanna B. Bowman, provided essential feedback on the manuscript. Z.Y.W. also thanks Anthony F. Iommi for valuable help.

Authorship Contributions

Participated in research design: Weinberg, Zajac, Puthenveedu.
Conducted experiments: Weinberg, Zajac, Puthenveedu.
Contributed new reagents or analytic tools: Phan, Shiwarski.
Performed data analysis: Weinberg, Zajac, Phan, Puthenveedu.
Wrote or contributed to the writing of the manuscript: Weinberg, Zajac, Puthenveedu.

References

Aguet F, Antonescu CN, Mettlen M, Schmid SL, and Danuser G (2013) Advances in analysis of low signal-to-noise images link dynamin and AP2 to the functions of an endocytic checkpoint. *Dev Cell* **26**:279–291.

Azzi M, Charest PG, Angers S, Rousseau G, Kohout T, Bouvier M, and Piñeyro G (2003) Beta-arrestin-mediated activation of MAPK by inverse agonists reveals distinct active conformations for G protein-coupled receptors. *Proc Natl Acad Sci USA* **100**:11406–11411.

Belcheva MM, Clark AL, Haas PD, Serna JS, Hahn JW, Kiss A, and Coscia CJ (2005) Mu and kappa opioid receptors activate ERK/MAPK via different protein kinase C isoforms and secondary messengers in astrocytes. *J Biol Chem* **280**:27662–27669.

Bowman SL, Shiwarski DJ, and Puthenveedu MA (2016) Distinct G protein-coupled receptor recycling pathways allow spatial control of downstream G protein signaling. *J Cell Biol* **214**:797–806.

Bradley SJ and Tobin AB (2016) Design of Next-Generation G Protein–Coupled Receptor Drugs: Linking Novel Pharmacology and In Vivo Animal Models. *Annu Rev Pharmacol Toxicol* **56**:535–559.

Chang SD and Bruchas MR (2014) Functional selectivity at GPCRs: new opportunities in psychiatric drug discovery. *Neuropsychopharmacology* **39**:248–249.

Cocucci E, Gaudin R, and Kirchhausen T (2014) Dynamin recruitment and membrane scission at the neck of a clathrin-coated pit. *Mol Biol Cell* **25**:3595–3609.

Daigle TL, Kwok ML, and Mackie K (2008) Regulation of CB1 cannabinoid receptor internalization by a promiscuous phosphorylation-dependent mechanism. *J Neurochem* **106**:70–82.

Delgado-Peraza F, Ahn KH, Nogueras-Ortiz C, Mungrue IN, Mackie K, Kendall DA, and Yudowski GA (2016) Mechanisms of Biased β-Arrestin-Mediated Signaling Downstream from the Cannabinoid 1 Receptor. *Mol Pharmacol* **89**:618–629.

DeWire SM, Ahn S, Lefkowitz RJ, and Shenoy SK (2007) Beta-arrestins and cell signaling. *Annu Rev Physiol* **69**:483–510.

DiPilato LM, Cheng X, and Zhang J (2004) Fluorescent indicators of cAMP and Epac activation reveal differential dynamics of cAMP signaling within discrete subcellular compartments. *Proc Natl Acad Sci USA* **101**:16513–16518.

Doll C, Konietzko J, Pöll F, Koch T, Höllt V, and Schulz S (2011) Agonist-selective patterns of μ-opioid receptor phosphorylation revealed by phosphosite-specific antibodies. *Br J Pharmacol* **164**:298–307.

Doll C, Pöll F, Peuker K, Loktev A, Glück L, and Schulz S (2012) Deciphering μ-opioid receptor phosphorylation and dephosphorylation in HEK293 cells. *Br J Pharmacol* **167**:1259–1270.

Doyon JB, Zeitler B, Cheng J, Cheng AT, Cherone JM, Santiago Y, Lee AH, Vo TD, Doyon Y, Miller JC, et al. (2011) Rapid and efficient clathrin-mediated endocytosis revealed in genome-edited mammalian cells. *Nat Cell Biol* **13**:331–337.

Dunn HA, Chahal HS, Caetano FA, Holmes KD, Yuan GY, Parikh R, Heit B, and Ferguson SSG (2016) PSD-95 regulates CRFR1 localization, trafficking and β-arrestin2 recruitment. *Cell Signal* **28**:531–540.

Dunn HA and Ferguson SSG (2015) PDZ Protein Regulation of G Protein-Coupled Receptor Trafficking and Signaling Pathways. *Mol Pharmacol* **88**:624–639.

Eichel K, Jullie D, and von Zastrow M (2016) β-Arrestin drives MAP kinase signalling from clathrin-coated structures after GPCR dissociation. *Nat Cell Biol* **18**:303–310.

Ferrandon S, Feinstein TN, Castro M, Wang B, Bouley R, Potts JT, Gardella TJ, and Vilardaga J-P (2009) Sustained cyclic AMP production by parathyroid hormone receptor endocytosis. *Nat Chem Biol* **5**:734–742.

Flores-Otero J, Ahn KH, Delgado-Peraza F, Mackie K, Kendall DA, and Yudowski GA (2014) Ligand-specific endocytic dwell times control functional selectivity of the cannabinoid receptor 1. *Nat Comms* **5**:4589.

Fritz RD, Letzelter M, Reimann A, Martin K, Fusco L, Ritsma L, Ponsioen B, Fluri E, Schulte-Merker S, van Rheenen J, et al. (2013) A versatile toolkit to produce sensitive FRET biosensors to visualize signaling in time and space. *Sci Signal* **6**:rs12.

Goodman OB, Krupnick JG, Santini F, Gurevich VV, Penn RB, Gagnon AW, Keen JH, and Benovic JL (1996) Beta-arrestin acts as a clathrin adaptor in endocytosis of the beta2-adrenergic receptor. *Nature* **383**:447–450.

Grassart A, Cheng AT, Hong SH, Zhang F, Zenzer N, Feng Y, Briner DM, Davis GD, Malkov D, and Drubin DG (2014) Actin and dynamin2 dynamics and interplay during clathrin-mediated endocytosis. *J Cell Biol* **205**:721–735.

Gurevich VV and Gurevich EV (2014) Extensive shape shifting underlies functional versatility of arrestins. *Curr Opin Cell Biol* **27**:1–9.

Halls ML, Yeatman HR, Nowell CJ, Thompson GL, Gondin AB, Civciristov S, Bunnett NW, Lambert NA, Poole DP, and Canals M (2016) Plasma membrane localization of the μ-opioid receptor controls spatiotemporal signaling. *Sci Signal* **9**:ra16.

Henry AG, Hislop JN, Grove J, Thorn K, Marsh M, and von Zastrow M (2012) Regulation of endocytic clathrin dynamics by cargo ubiquitination. *Dev Cell* **23**:519–532.

Hong SH, Cortesio CL, and Drubin DG (2015) Machine-learning-based analysis in genome-edited cells reveals the efficiency of clathrin-mediated endocytosis. *Cell Rep* **12**:2121–2130.

Irannejad R, Tomshine JC, Tomshine JR, Chevalier M, Mahoney JP, Steyaert J, Rasmussen SGF, Sunahara RK, El-Samad H, and Huang B, et al. (2013) Conformational biosensors reveal GPCR signalling from endosomes. *Nature* **495**:534–538.

Jean-Alphonse F, Bowersox S, Chen S, Beard G, Puthenveedu MA, and Hanyaloglu AC (2014) Spatially restricted G protein-coupled receptor activity via divergent endocytic compartments. *J Biol Chem* **289**:3960–3977.

Keith DE, Murray SR, Zaki PA, Chu PC, Lissin DV, Kang L, Evans CJ, and von Zastrow M (1996) Morphine activates opioid receptors without causing their rapid internalization. *J Biol Chem* **271**:19021–19024.

Kenakin T (2015) The Effective Application of Biased Signaling to New Drug Discovery. *Mol Pharmacol* **88**:1055–1061.

Lampe M, Pierre F, Al-Sabah S, Krasel C, and Merrifield CJ (2014) Dual single-scission event analysis of constitutive transferrin receptor (TfR) endocytosis and ligand-triggered β2-adrenergic receptor (β2AR) or Mu-opioid receptor (MOR) endocytosis. *Mol Biol Cell* **25**:3070–3080.

Law P-Y, Reggio PH, and Loh HH (2013) Opioid receptors: toward separation of analgesic from undesirable effects. *Trends Biochem Sci* **38**:275–282.

Lee H-J and Zheng JJ (2010) PDZ domains and their binding partners: structure, specificity, and modification. *Cell Commun Signal* **8**:8.

Lee M-H, Appleton KM, Strungs EG, Kwon JY, Morinelli TA, Peterson YK, Laporte SA, and Luttrell LM (2016) The conformational signature of β-arrestin2 predicts its trafficking and signalling functions. *Nature* **531**:665–668.

Lefkowitz RJ, Wisler JW, Xiao K, and Thomsen AR (2014) Recent developments in biased agonism. *Curr Opin Cell Biol* **27**:18–24.

Lin X, Wang Q, Ji J, and Yu L-C (2010) Role of MEK-ERK pathway in morphine-induced conditioned place preference in ventral tegmental area of rats. *J Neurosci Res* **88**:1595–1604.
Liu AP, Aguet F, Danuser G, and Schmid SL (2010) Local clustering of transferrin receptors promotes clathrin-coated pit initiation. *J Cell Biol* **191**:1381–1393.
Loerke D, Mettlen M, Yarar D, Jaqaman K, Jaqaman H, Danuser G, and Schmid SL (2009) Cargo and dynamin regulate clathrin-coated pit maturation. *PLoS Biol* **7**: e57.
Luttrell LM, Ferguson SS, Daaka Y, Miller WE, Maudsley S, Rocca Della GJ, Lin F, Kawakatsu H, Owada K, Luttrell DK, et al. (1999) Beta-arrestin-dependent formation of beta2 adrenergic receptor-Src protein kinase complexes. *Science* **283**: 655–661.
Luttrell LM and Lefkowitz RJ (2002) The role of beta-arrestins in the termination and transduction of G-protein-coupled receptor signals. *J Cell Sci* **115**:455–465.
Luttrell LM, Maudsley S, and Bohn LM (2015) Fulfilling the promise of "biased" G protein-coupled receptor agonism. *Mol Pharmacol* **88**:579–588.
Macey TA, Bobeck EN, Hegarty DM, Aicher SA, Ingram SL, and Morgan MM (2009) Extracellular signal-regulated kinase 1/2 activation counteracts morphine tolerance in the periaqueductal gray of the rat. *J Pharmacol Exp Ther* **331**:412–418.
Macia E, Ehrlich M, Massol R, Boucrot E, Brunner C, and Kirchhausen T (2006) Dynasore, a Cell-Permeable Inhibitor of Dynamin. *Dev Cell* **10**:839–850.
Manglik A, Lin H, Aryal DK, McCorvy JD, Dengler D, Corder G, Levit A, Kling RC, Bernat V, and Hübner H, et al. (2016) Structure-based discovery of opioid analgesics with reduced side effects. *Nature* **537**:185–190.
McMahon HT and Boucrot E (2011) Molecular mechanism and physiological functions of clathrin-mediated endocytosis. *Nat Rev Mol Cell Biol* **12**:517–533.
McPherson J, Rivero G, Baptist M, Llorente J, Al-Sabah S, Krasel C, Dewey WL, Bailey CP, Rosethorne EM, Charlton SJ, et al. (2010) μ-opioid receptors: correlation of agonist efficacy for signalling with ability to activate internalization. *Mol Pharmacol* **78**:756–766.
Mettlen M and Danuser G (2014) Imaging and modeling the dynamics of clathrin-mediated endocytosis. *Cold Spring Harb Perspect Biol* **6**: a017038. 10.1101/cshperspect.a017038.
Nobles KN, Xiao K, Ahn S, Shukla AK, Lam CM, Rajagopal S, Strachan RT, Huang TY, Bressler EA, Hara MR, et al. (2011) Distinct phosphorylation sites on the β(2)-adrenergic receptor establish a barcode that encodes differential functions of β-arrestin. *Sci Signal* **4**:ra51.
Nuber S, Zabel U, Lorenz K, Nuber A, Milligan G, Tobin AB, Lohse MJ, and Hoffmann C (2016) β-Arrestin biosensors reveal a rapid, receptor-dependent activation/deactivation cycle. *Nature* **531**:661–664.
Paasche JD, Attramadal T, Kristiansen K, Oksvold MP, Johansen HK, Huitfeldt HS, Dahl SG, and Attramadal H (2005) Subtype-specific sorting of the ETA endothelin receptor by a novel endocytic recycling signal for G protein-coupled receptors. *Mol Pharmacol* **67**:1581–1590.
Pierce KL, Premont RT, and Lefkowitz RJ (2002) Seven-transmembrane receptors. *Nat Rev Mol Cell Biol* **3**:639-50.
Premont RT and Gainetdinov RR (2007) Physiological roles of G protein-coupled receptor kinases and arrestins. *Annu Rev Physiol* **69**:511–534.
Puthenveedu MA and von Zastrow M (2006) Cargo regulates clathrin-coated pit dynamics. *Cell* **127**:113–124.
Raehal KM and Bohn LM (2014) β-arrestins: regulatory role and therapeutic potential in opioid and cannabinoid receptor-mediated analgesia. *Handb Exp Pharmacol* **219**:427–443.
Raehal KM, Schmid CL, Groer CE, and Bohn LM (2011) Functional selectivity at the μ-opioid receptor: implications for understanding opioid analgesia and tolerance. *Pharmacol Rev* **63**:1001–1019.
Rivero G, Llorente J, McPherson J, Cooke A, Mundell SJ, McArdle CA, Rosethorne EM, Charlton SJ, Krasel C, Bailey CP, et al. (2012) Endomorphin-2: A Biased Agonist at the -Opioid Receptor. *Mol Pharmacol* **82**:178–188.
Romero G, von Zastrow M, and Friedman PA (2011) Role of PDZ proteins in regulating trafficking, signaling, and function of GPCRs: means, motif, and opportunity. *Adv Pharmacol* **62**:279–314.
Shenoy SK and Lefkowitz RJ (2011) β-Arrestin-mediated receptor trafficking and signal transduction. *Trends Pharmacol Sci* **32**:521–533.
Smith TH, Blume LC, Straiker A, Cox JO, David BG, McVoy JRS, Sayers KW, Poklis JL, Abdullah RA, Egertová M, et al. (2015) Cannabinoid receptor-interacting protein 1a modulates CB1 receptor signaling and regulation. *Mol Pharmacol* **87**: 747–765.
Soohoo AL and Puthenveedu MA (2013) Divergent modes for cargo-mediated control of clathrin-coated pit dynamics. *Mol Biol Cell* **24**:1725–1734.
Sternini C, Spann M, Anton B, Keith, JrDE, Bunnett NW, von Zastrow M, Evans C, and Brecha NC (1996) Agonist-selective endocytosis of mu opioid receptor by neurons in vivo. *Proc Natl Acad Sci USA* **93**:9241–9246.
Strungs EG and Luttrell LM (2014) Arrestin-dependent activation of ERK and Src family kinases. *Handb Exp Pharmacol* **219**:225–257.
Taylor MJ, Perrais D, and Merrifield CJ (2011) A high precision survey of the molecular dynamics of mammalian clathrin-mediated endocytosis. *PLoS Biol* **9**: e1000604.
Thompson GL, Kelly E, Christopoulos A, and Canals M (2015) Novel GPCR paradigms at the μ-opioid receptor. *Br J Pharmacol* **172**:287–296.
Tobin AB, Butcher AJ, and Kong KC (2008) Location, location, location...site-specific GPCR phosphorylation offers a mechanism for cell-type-specific signalling. *Trends Pharmacol Sci* **29**:413–420.
Traub LM and Bonifacino JS (2013) Cargo recognition in clathrin-mediated endocytosis. *Cold Spring Harb Perspect Biol* **5**:a016790.
Tsvetanova NG and von Zastrow M (2014) Spatial encoding of cyclic AMP signaling specificity by GPCR endocytosis. *Nat Chem Biol* **10**:1061–1065.
Urban JD, Clarke WP, von Zastrow M, Nichols DE, Kobilka B, Weinstein H, Javitch JA, Roth BL, Christopoulos A, Sexton PM, et al. (2007) Functional selectivity and classical concepts of quantitative pharmacology. *J Pharmacol Exp Ther* **320**:1–13.
Violin JD, Crombie AL, Soergel DG, and Lark MW (2014) Biased ligands at G-protein-coupled receptors: promise and progress. *Trends Pharmacol Sci* **35**: 308–316.
Walther C, Caetano FA, Dunn HA, and Ferguson SSG (2015) PDZK1/NHERF3 differentially regulates corticotropin-releasing factor receptor 1 and serotonin 2A receptor signaling and endocytosis. *Cell Signal* **27**:519–531.
Whistler JL and von Zastrow M (1998) Morphine-activated opioid receptors elude desensitization by beta-arrestin. *Proc Natl Acad Sci U S A* **95**:9914–9919.
Williams JT, Ingram SL, Henderson G, Chavkin C, von Zastrow M, Schulz S, Koch T, Evans CJ, and Christie MJ (2013) Regulation of μ-opioid receptors: desensitization, phosphorylation, internalization, and tolerance. *Pharmacol Rev* **65**: 223–254.
Wolfe BL and Trejo J (2007) Clathrin-dependent mechanisms of G protein-coupled receptor endocytosis. *Traffic* **8**:462–470.
Xiao K, McClatchy DB, Shukla AK, Zhao Y, Chen M, Shenoy SK, Yates JR, and Lefkowitz RJ (2007) Functional specialization of beta-arrestin interactions revealed by proteomic analysis. *Proc Natl Acad Sci USA* **104**:12011–12016.
Yang X, Zheng J, Xiong Y, Shen H, Sun L, Huang Y, Sun C, Li Y, and He J (2010) Beta-2 adrenergic receptor mediated ERK activation is regulated by interaction with MAGI-3. *FEBS Lett* **584**:2207–2212.
Yu Y, Zhang L, Yin X, Sun H, Uhl GR, and Wang JB (1997) Mu opioid receptor phosphorylation, desensitization, and ligand efficacy. *J Biol Chem* **272**: 28869–28874.
Zheng H, Loh HH, and Law P-Y (2008) Beta-arrestin-dependent mu-opioid receptor-activated extracellular signal-regulated kinases (ERKs) Translocate to Nucleus in Contrast to G protein-dependent ERK activation. *Mol Pharmacol* **73**:178–190.
Zhou L and Bohn LM (2014) Functional selectivity of GPCR signaling in animals. *Curr Opin Cell Biol* **27**:102–108.
Zindel D, Butcher AJ, Al-Sabah S, Lanzerstorfer P, Weghuber J, Tobin AB, Bünemann M, and Krasel C (2015) Engineered Hyperphosphorylation of the β2-Adrenoceptor Prolongs Arrestin-3 Binding and Induces Arrestin Internalization. *Mol Pharmacol* **87**:349–362.

Address correspondence to: Manojkumar Puthenveedu, Department of Biological Sciences, 4400 Fifth Avenue MI202, Carnegie Mellon University, Pittsburgh, PA 15213. E-mail: map3@andrew.cmu.edu

Title: Sequence-specific regulation of endocytic lifetimes modulates arrestin-mediated signaling at the μ opioid receptor

Authors: Zara Y. Weinberg, Amanda S. Zajac, Tiffany Phan, Daniel J. Shiwarski, Manojkumar A. Puthenveedu

Journal: Molecular Pharmacology

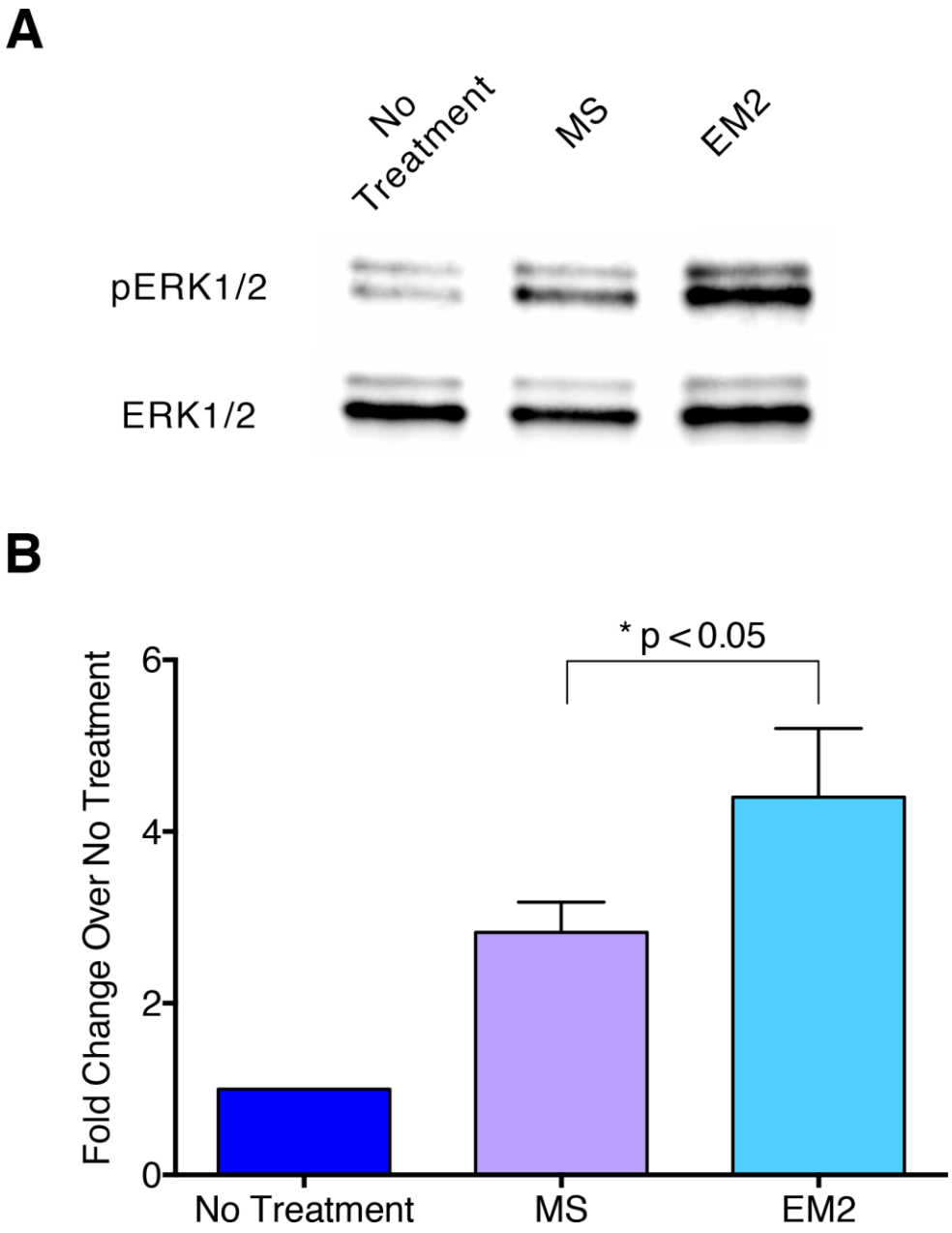

Supplemental Figure 1: EM2 causes a greater increase in phospho-ERK1/2 compared to morphine when assayed via immunotblot. A) Representative immunoblot for phospho-

ERK1/2 in cells expressing WT μR and treated with either water, morphine (10μM), or EM2 for 5 minutes. Top row is phospho-ERK (Thr202), bottom row is ERK1/2 as loading control. 2) Quantification of 3 experiments, each replicated three times for a total of 9 blots. Bands were normalized to no treatment control, and then averaged across blots. A significant effect of treatment was seen via a repeated-measures oneway ANOVA (** $p < 0.01$), with a significant difference seen between morphine- and EM2-dependent response.

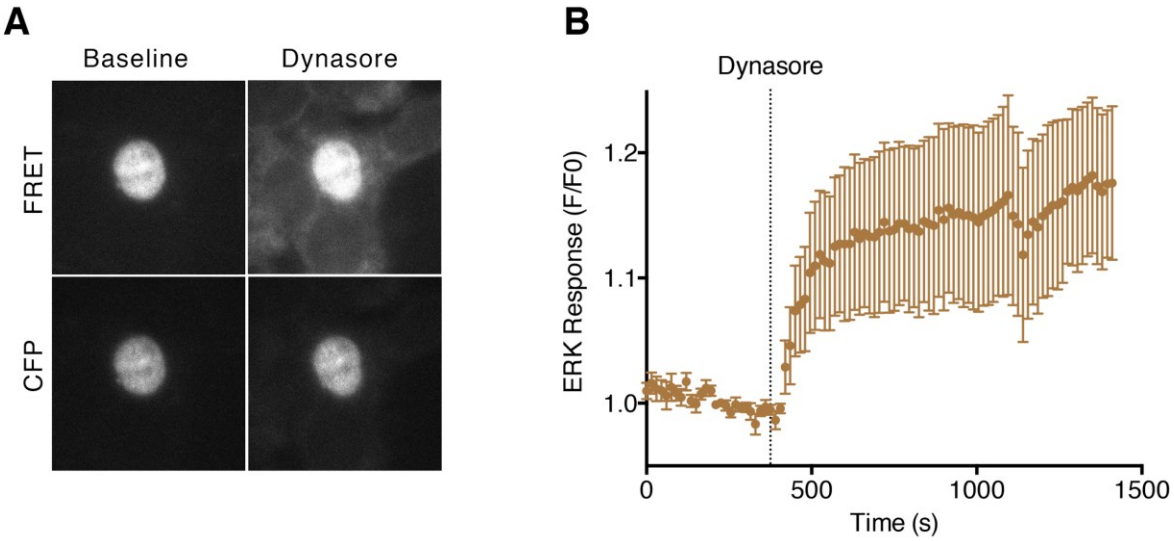

Supplemental Figure 2: Dynasore shows autofluorescence in the YFP channel. A) Representative images from before and after dynasore (40µM) addition to cell expressing nEKAR sensor. Top row: FRET channel (405nm laser excitation, collection through 530lp emission filter), bottom row: CFP channel (405nm laser excitation, collection through 470/50 emission filter) . Left side is after 5 minutes of no treatment, right side is after 5 minutes of dynasore treatment. Note accumulation of fluorescence on surrounding cells that don't express sensor, seen only in FRET channel. B) FRET/CFP ratio was calculated per methods and normalized to untreated baseline. Average ratio across cells (n=5) is shown on the graph, showing a dramatic increase in FRET signal. This is due to autofluorescence and not ERK activation, as dynasore alone has minimal effect on phospho-ERK levels (see Figure 5, C and E).